

Department of Physics
Kyoto University

KUNS 1398
YITP-96-20
September 15, 2021

Innermost Stable Circular Orbit of Coalescing Neutron Star-Black Hole Binary

— Generalized Pseudo-Newtonian Potential Approach —

Keisuke Taniguchi *

Department of Physics, Kyoto University, Kyoto 606-01, Japan

Takashi Nakamura

Yukawa Institute for Theoretical Physics, Kyoto University, Kyoto 606-01, Japan

To appear in *Progress of Theoretical Physics, Vol.96 No.4*

Abstract

The innermost stable circular orbits (ISCO) of coalescing neutron star-black hole binary are studied taking into account both the tidal and relativistic effects. We adopt the generalized pseudo-Newtonian potential to mimic the general relativistic effects of gravitation. It is found that the separation of the neutron star and the black hole at the innermost stable circular orbit is greater than that obtained by using either the Newtonian potential (i.e. the case in which only the tidal interaction is included.) or the second post-Newtonian equation of motion of point mass (i.e. the case in which the effect of general relativity is taken into account but the tidal force is neglected.). In equal mass cases, it is found that for $\bar{a}/m_1 \gtrsim 3.5$ with \bar{a} and m_1 being the mean radius and the mass of the neutron star, the tidal effect dominates the stability of the binary system while for $\bar{a}/m_1 \lesssim 3.5$, the relativistic effect, i.e. the fact that the interaction potential has unstable orbit, does. The effect of the circulation is also studied by comparing the Roche ellipsoids (REs) with

* e-mail: taniguci@tap.scphys.kyoto-u.ac.jp

the irrotational Roche-Riemann ellipsoids (IRREs). In the IRREs case, which are believed to be the case of coalescing binary neutron stars, it is found that in the equal mass binary case, the orbital frequency is 495Hz at the ISCO.

PACS number(s): 04.30.Db

I. INTRODUCTION

The laser interferometers like LIGO [1], VIRGO [2], GEO [3] and TAMA [4] are currently constructed and the detection of gravitational waves is expected at the end of this century. One of the most important sources of gravitational waves for these detectors is coalescing binary compact stars such as NS-NS, NS-BH and BH-BH binaries. Each mass, each spin and the distance of the binary can be determined by applying the matched filter techniques [5] to the gravitational wave form of the so-called last three minutes of the binary [6]. In the end of the last three minutes two compact stars coalesce and nonlinear character of the gravity and the tidal effects become important, which will be the most exciting part of the coalescing event.

It is known from the study of orbits of a test particle in the Schwarzschild metric that the innermost stable circular orbit (ISCO) exists at $r = 6M$. For binary cases, Kidder, Will, & Wiseman [7] investigated a point-mass binary using second post-Newtonian equation of motion, and found that the ISCO of the comparable mass binary is at $r_{gr} \simeq 7M_{tot}$ where r_{gr} is the separation of the binary in the Schwarzschild like radial coordinate.

As for the tidal effects, Chandrasekhar [8] studied the Roche limit by using Newtonian gravity and treating binary systems as incompressible homogeneous ellipsoids. He found that the stars are tidally disrupted before contact at $r_t = (2.25M_{tot}/\rho)^{1/3}$ for equal mass binary where ρ is the constant density of ellipsoids. For the typical neutron star with $M_{tot} = 2.8M_{\odot}$ and $\rho = 1 \times 10^{15} \text{g/cm}^3$, r_t becomes $5.6M_{tot}$.

Recently Lai, Rasio, & Shapiro [9] [10] have investigated the binary consist of finite size compressible stars using approximate equilibria. In a series of their papers, they took into account the effect of the quadrupole order deviation of stars and found that the hydrodynamic instability occurs at $r_h = 6 \sim 7.5M_{tot}$ for $n = 0.5$ polytropic neutron star with the radius $R_0 = 2.5M_{tot}$.

In order to know at what radius the final merging phase begins, all three effects, that is, the general relativistic, tidal and hydrodynamic effects should be taken into account simultaneously since r_{gr} , r_t and r_h have similar values of $\sim 7M_{tot}$. For this purpose we must solve the fully general relativistic equations, which is a difficult 3D problem in numerical relativity [11] although the partly general relativistic results have already been presented [12] [13]. To know the qualitative feature of the ISCOs we will use various approximations to calculate equilibria of the binary in this paper. The reward is that all the calculations can be done analytically so that our results will contribute some physical aspects to the final understanding of the ISCO.

In this paper, we will solve the Roche problem [8] as a model of the binary that consists of a finite size star and a point-like gravity source. A gravitational potential which has unstable circular orbits will be used as an interaction potential of the binary. Specifically, we generalize the pseudo-Newtonian potential proposed by Paczyński & Wiita [14] to mimic the general relativistic effects. We think that this model mimics a neutron star-black hole binary, and describes its qualitative behavior.

This paper is organized as follows. In §2 the basic equations necessary for constructing equilibrium configurations of the Roche ellipsoids (REs) and the Roche-Riemann ellipsoids (RREs) [15] are derived in the case that the interaction potential is general. In §3 circular orbits of the neutron star-black hole binary are calculated using the generalized pseudo-

Newtonian potential to mimic the effects of general relativity and the results are shown in §4. In §5 our results are compared with those using the Newtonian potential and the second order post-Newtonian equation of motion. We use the units of $c = G = 1$ through this paper.

II. GENERALIZED ROCHE-RIEMANN ELLIPSOIDS

We first regard the black hole as a point particle of mass m_2 and denote the gravitational potential by the black hole as $V_2(r)$. To mimic the effects of general relativity by $V_2(r)$, we do not fix the form of $V_2(r)$ at the moment. Next we treat the neutron star as an incompressible, homogeneous ellipsoid of the semi-axes a_1, a_2 and a_3 , mass m_1 and the density ρ_1 . We treat the self-gravity of the neutron star (V_1) as Newtonian. Although for mathematical convenience we assume the incompressibility for the equation of state, the effect of the compressibility can be easily taken into account in an approximate way [9]. Following Chandrasekhar [8], we call the neutron star the primary and the black hole the secondary.

A. Second Virial Equations

We use the tensor virial method [8], and derive the equations necessary for constructing equilibrium figures of this system. Choose a coordinate system such that the origin is at the center of mass of the primary, the x_1 -axis points to the center of mass of the secondary, and x_3 -axis coincides with the direction of the angular velocity of the binary $\boldsymbol{\Omega}$. In the frame of reference rotating with $\boldsymbol{\Omega}$, the Euler equations of the primary are written as

$$\rho_1 \frac{du_i}{dt} = -\frac{\partial P}{\partial x_i} + \rho_1 \frac{\partial}{\partial x_i} \left[V_1 + V_2 + \frac{1}{2} \Omega^2 \left\{ \left(\frac{m_2 R}{m_1 + m_2} - x_1 \right)^2 + x_2^2 \right\} \right] + 2\rho_1 \Omega \epsilon_{il3} u_l, \quad (2.1)$$

where ρ_1, u_i, P and R are the density, the internal velocity, the pressure and the separation between the neutron star and the black hole, respectively.

Let us expand the interaction potential V_2 in power series of x_k up to the second order. This approximation is justified if R is much larger than a_1, a_2 and a_3 . We assume that the potential V_2 is spherically symmetric so that it depends only on the distance r from the center of mass of the secondary as

$$V_2 = V_2(r), \quad (2.2)$$

where r is given by

$$r = \left\{ (R - x_1)^2 + x_2^2 + x_3^2 \right\}^{1/2}. \quad (2.3)$$

The expansion of $V_2(r)$ becomes

$$V_2 = (V_2)_0 - \left(\frac{\partial V_2}{\partial r} \right)_0 x_1 + \frac{1}{2} \left(\frac{\partial^2 V_2}{\partial r^2} \right)_0 x_1^2 + \frac{1}{2R} \left(\frac{\partial V_2}{\partial r} \right)_0 (x_2^2 + x_3^2), \quad (2.4)$$

where the subscript 0 denotes the derivatives at the origin of the coordinates. In the case of the circular orbit, we have from the force balance at the center

$$\frac{m_2 R}{m_1 + m_2} \Omega^2 = - \left(\frac{\partial V_2}{\partial r} \right)_0 (1 + \delta), \quad (2.5)$$

where δ is the quadrupole term of the interaction potential [9].

Substituting Eqs.(2.4) and (2.5) into Eq.(2.1), we have

$$\begin{aligned} \rho_1 \frac{du_i}{dt} = & - \frac{\partial P}{\partial x_i} + \rho_1 \frac{\partial}{\partial x_i} \left[V_1 + \delta \left(\frac{\partial V_2}{\partial r} \right)_0 x_1 + \frac{1}{2} \Omega^2 (x_1^2 + x_2^2) + \frac{1}{2} \left(\frac{\partial^2 V_2}{\partial r^2} \right)_0 x_1^2 \right. \\ & \left. + \frac{1}{2R} \left(\frac{\partial V_2}{\partial r} \right)_0 (x_2^2 + x_3^2) \right] + 2\rho_1 \Omega \epsilon_{il3} u_l. \end{aligned} \quad (2.6)$$

Multiplying x_j to Eq.(2.6) and integrating over the volume of the primary, we have

$$\begin{aligned} \frac{d}{dt} \int \rho_1 u_i x_j d^3 \mathbf{x} = & 2T_{ij} + W_{ij} + \left\{ \Omega^2 + \left(\frac{\partial^2 V_2}{\partial r^2} \right)_0 \right\} \delta_{1i} I_{1j} \\ & + \left\{ \Omega^2 + \frac{1}{R} \left(\frac{\partial V_2}{\partial r} \right)_0 \right\} \delta_{2i} I_{2j} + \frac{1}{R} \left(\frac{\partial V_2}{\partial r} \right)_0 \delta_{3i} I_{3j} \\ & + 2\Omega \epsilon_{il3} \int \rho_1 u_l x_j d^3 \mathbf{x} + \delta_{ij} \Pi, \end{aligned} \quad (2.7)$$

where

$$T_{ij} \equiv \frac{1}{2} \int \rho_1 u_i u_j d^3 \mathbf{x} : \text{Kinetic Energy Tensor}, \quad (2.8)$$

$$W_{ij} \equiv \int \rho_1 \frac{\partial V_1}{\partial x_i} x_j d^3 \mathbf{x} : \text{Potential Energy Tensor}, \quad (2.9)$$

$$I_{ij} \equiv \int \rho_1 x_i x_j d^3 \mathbf{x} : \text{Moment of Inertia Tensor}, \quad (2.10)$$

and

$$\Pi \equiv \int P d^3 \mathbf{x}. \quad (2.11)$$

In Eq.(2.7) there is no terms related to δ . Since it is possible to take the coordinate system comoving with the center of mass of the binary system, the term proportional to δ in Eq.(2.6) vanishes when we integrate over the volume of the primary. Eq.(2.7) is the basic equation to construct the equilibrium figures of the Roche ellipsoids (REs) and the Roche-Riemann ellipsoids (RREs) for the general potential $V_2(r)$.

B. Equilibrium Roche-Riemann Sequence

In this subsection, we show how to construct the equilibrium figures of the RREs. The Roche-Riemann ellipsoid is the equilibrium in which the shape of the primary does not

change in the rotating frame although the uniform vorticity exists inside the primary. We restrict the problem to the simplest case where the uniform vorticity of the primary is parallel to the rotation axis, i.e. the primary is the Riemann S-type ellipsoid [8].

We set the coordinate axes to coincide with the principal axes of the primary. For the uniform vorticity ζ , the internal velocity u_i in the rotating frame is given by

$$u_1 = Q_1 x_2, \quad (2.12)$$

$$u_2 = Q_2 x_1, \quad (2.13)$$

and

$$u_3 = 0, \quad (2.14)$$

where

$$Q_1 = -\frac{a_1^2}{a_1^2 + a_2^2} \zeta \quad (2.15)$$

and

$$Q_2 = \frac{a_2^2}{a_1^2 + a_2^2} \zeta. \quad (2.16)$$

For the stationary equilibrium, Eq.(2.7) is rewritten as

$$\begin{aligned} Q_{ik} Q_{jl} I_{kl} + W_{ij} + \left\{ \Omega^2 + \left(\frac{\partial^2 V_2}{\partial r^2} \right)_0 \right\} \delta_{1i} I_{1j} + \left\{ \Omega^2 + \frac{1}{R} \left(\frac{\partial V_2}{\partial r} \right)_0 \right\} \delta_{2i} I_{2j} \\ + \frac{1}{R} \left(\frac{\partial V_2}{\partial r} \right)_0 \delta_{3i} I_{3j} + 2\Omega \epsilon_{il3} Q_{lk} I_{kj} = -\delta_{ij} \Pi, \end{aligned} \quad (2.17)$$

where Q_{ij} is not zero only for

$$Q_{12} = Q_1, \quad (2.18)$$

$$Q_{21} = Q_2. \quad (2.19)$$

Eq.(2.17) has only diagonal components as

$$Q_1^2 I_{22} + W_{11} + \left\{ \Omega^2 + \left(\frac{\partial^2 V_2}{\partial r^2} \right)_0 \right\} I_{11} + 2\Omega Q_2 I_{11} = -\Pi, \quad (2.20)$$

$$Q_2^2 I_{11} + W_{22} + \left\{ \Omega^2 + \frac{1}{R} \left(\frac{\partial V_2}{\partial r} \right)_0 \right\} I_{22} - 2\Omega Q_1 I_{22} = -\Pi, \quad (2.21)$$

and

$$W_{33} + \frac{1}{R} \left(\frac{\partial V_2}{\partial r} \right)_0 I_{33} = -\Pi. \quad (2.22)$$

We assume for simplicity that the gravitational potential of the primary is Newtonian. In this case, the potential energy tensor and the moment of inertia tensor of the incompressible, homogeneous ellipsoids are calculated as

$$W_{ij} = -2\pi\rho_1 A_i I_{ij}, \quad (2.23)$$

and

$$I_{ij} = \frac{1}{5} m_1 a_i^2 \delta_{ij}, \quad (2.24)$$

where

$$A_i = a_1 a_2 a_3 \int_0^\infty \frac{du}{\Delta(a_i^2 + u)}, \quad (2.25)$$

and

$$\Delta^2 = (a_1^2 + u)(a_2^2 + u)(a_3^2 + u). \quad (2.26)$$

Eliminating Π from Eqs.(2.20)-(2.22), we have

$$\begin{aligned} \left[\left\{ 1 + 2 \frac{a_2^2}{a_1^2 + a_2^2} f_R + \left(\frac{a_1 a_2}{a_1^2 + a_2^2} f_R \right)^2 \right\} \Omega^2 + \left(\frac{\partial^2 V_2}{\partial r^2} \right)_0 \right] a_1^2 - \frac{1}{R} \left(\frac{\partial V_2}{\partial r} \right)_0 a_3^2 \\ = 2\pi\rho_1 (a_1^2 - a_3^2) B_{13} \end{aligned} \quad (2.27)$$

and

$$\begin{aligned} \left[\left\{ 1 + 2 \frac{a_1^2}{a_1^2 + a_2^2} f_R + \left(\frac{a_1 a_2}{a_1^2 + a_2^2} f_R \right)^2 \right\} \Omega^2 + \frac{1}{R} \left(\frac{\partial V_2}{\partial r} \right)_0 \right] a_2^2 - \frac{1}{R} \left(\frac{\partial V_2}{\partial r} \right)_0 a_3^2 \\ = 2\pi\rho_1 (a_2^2 - a_3^2) B_{23}, \end{aligned} \quad (2.28)$$

where

$$f_R \equiv \frac{\zeta}{\Omega} \quad (2.29)$$

and the following relations are used;

$$a_i^2 A_i - a_j^2 A_j = (a_i^2 - a_j^2) B_{ij}, \quad (2.30)$$

where

$$B_{ij} = a_1 a_2 a_3 \int_0^\infty \frac{u du}{\Delta(a_i^2 + u)(a_j^2 + u)}. \quad (2.31)$$

Now from Eq.(2.5) Ω is given by

$$\Omega^2 = -\frac{1+p}{R} \left(\frac{\partial V_2}{\partial r} \right)_0 (1+\delta) \quad \left(p \equiv \frac{m_1}{m_2} \right). \quad (2.32)$$

Dividing Eq.(2.27) by Eq.(2.28), we have the equation to determine the Roche-Riemann sequences as

$$\frac{\left[(1+p)(1+\delta) \left\{ 1 + 2 \frac{a_2^2}{a_1^2+a_2^2} f_R + \left(\frac{a_1 a_2}{a_1^2+a_2^2} f_R \right)^2 \right\} - R \left(\frac{\partial^2 V_2}{\partial r^2} \right)_0 / \left(\frac{\partial V_2}{\partial r} \right)_0 \right] a_1^2 + a_3^2}{\left[(1+p)(1+\delta) \left\{ 1 + 2 \frac{a_1^2}{a_1^2+a_2^2} f_R + \left(\frac{a_1 a_2}{a_1^2+a_2^2} f_R \right)^2 \right\} - 1 \right] a_2^2 + a_3^2} = \frac{(a_1^2 - a_3^2) B_{13}}{(a_2^2 - a_3^2) B_{23}}. \quad (2.33)$$

Using Eqs.(2.28) and (2.32), we can determine the orbital angular velocity Ω by

$$\frac{\Omega^2}{\pi \rho_1} = \frac{2(1+p)(1+\delta) (a_2^2 - a_3^2) B_{23}}{\left[(1+p)(1+\delta) \left\{ 1 + 2 \frac{a_1^2}{a_1^2+a_2^2} f_R + \left(\frac{a_1 a_2}{a_1^2+a_2^2} f_R \right)^2 \right\} - 1 \right] a_2^2 + a_3^2}. \quad (2.34)$$

Note that f_R is related to the circulation \mathcal{C} as

$$\mathcal{C} = \oint \mathbf{u}_{inertial} \cdot d\mathbf{l} = \pi a_1 a_2 (2 + f_R) \Omega, \quad (2.35)$$

where

$$\mathbf{u}_{inertial} = \begin{cases} (u_{inertial})_1 = (Q_1 - \Omega)x_2, \\ (u_{inertial})_2 = (Q_2 + \Omega)x_1 - \frac{R}{1+p}\Omega \\ (u_{inertial})_3 = 0. \end{cases} \quad (2.36)$$

If there is no viscosity inside the primary, the circulation should be conserved from Kelvin's circulation theorem.

C. Total Angular Momentum

The total energy and the total angular momentum of the binary are the decreasing functions of time since the gravitational waves are emitted. If the total angular momentum has its minimum at some separation of the binary, we regard this point as the ISCO [†]. The total angular momentum of our system which is the sum of the orbital and the spin angular momentum is given by

$$\begin{aligned} J_{tot} &= m_1 r_{cm}^2 \Omega + m_2 (R - r_{cm})^2 \Omega + I \Omega + \frac{2}{5} m_1 \frac{a_1^2 a_2^2}{a_1^2 + a_2^2} \zeta \\ &= \frac{m_1 m_2}{m_1 + m_2} R^2 \Omega \left\{ 1 + \frac{1}{5} (1+p) \frac{1}{R^2} \left(a_1^2 + a_2^2 + 2 \frac{a_1^2 a_2^2}{a_1^2 + a_2^2} f_R \right) \right\} \end{aligned} \quad (2.37)$$

where

[†]Lai, Rasio, & Shapiro show in appendix D of [9] that the true minimum point of the total energy coincides with that of the total angular momentum. Strictly speaking, if the rotation includes only to the quadrupole order, this coincidence fails. However the difference is as small as the numerical accuracy [9].

$$r_{cm} = \frac{m_2 R}{m_1 + m_2}. \quad (2.38)$$

The first term in the braces of the right hand side of Eq.(2.37) comes from the orbital angular momentum of the binary system and the second does from the spin angular momentum of the primary.

III. GENERALIZED PSEUDO-NEWTONIAN POTENTIAL

There are variety of choices of $V_2(r)$ to mimic the general relativistic effects of the gravitation. We generalize the so-called pseudo-Newtonian potential proposed by Paczyński & Wiita [14] originally. This potential fits the effective potential of the Schwarzschild black hole quite well as we will show later. We will use the generalized pseudo-Newtonian potential defined by

$$V_2(r) = \frac{m_2}{r - r_{pseudo}}, \quad (3.1)$$

$$r_{pseudo} = r_s \{1 + g(p)\}, \quad (3.2)$$

$$g(p) = \frac{7.49p}{6(1+p)^2} - \frac{10.4p^2}{3(1+p)^4} + \frac{29.3p^3}{6(1+p)^6}, \quad (3.3)$$

$$r_s \equiv \frac{2GM_{tot}}{c^2}, \quad (3.4)$$

$$M_{tot} = m_1 + m_2, \quad (3.5)$$

where $p = m_1/m_2$ and $g(p)$ is the special term to fit the ISCOs of the hybrid second post-Newtonian calculations by Kidder, Will, & Wiseman [7]. For $p = 0$, the generalized pseudo-Newtonian potential agrees with the pseudo-Newtonian potential proposed by Paczyński & Wiita [14].

Fig.1(a) shows effective potentials (solid lines) and locations of circular orbits (dots) in our generalized pseudo-Newtonian potential ($p = 0$ & $r_{pseudo} = r_s$) and in the Schwarzschild metric. Although by this choice of the parameter ($r_{pseudo} = r_s$), the locations of the ISCOs in the generalized pseudo-Newtonian potential agree with those in the Schwarzschild metric, the angular momenta at the ISCO are different, that is, the angular momentum in the generalized pseudo-Newtonian potential (J_{pseudo}) for $p = 0$ is $(9/8)^{1/2}$ times larger than that in the Schwarzschild metric (J_{Sch}) at the ISCO. Therefore in Fig.1(a) and (b) we compare circular orbits with different angular momentum related as

$$J_{pseudo} = \left(\frac{9}{8}\right)^{1/2} J_{Sch}. \quad (3.6)$$

From Fig.1(b) we see that the radii of the circular orbits of the generalized pseudo-Newtonian potential agrees with those of the effective potential around Schwarzschild black hole within 10% accuracy near the ISCO. This is the reason why we believe that our generalized pseudo-Newtonian potential expresses the effect of general relativity within 10% or so.

Using Eq.(3.1) and Eq.(2.32), we can rewrite Eq.(2.34) as

$$\frac{p^2 r_s^3 (\bar{a}/m_1)^3}{12(1+p)^3 R(R-r_{pseudo})^2} - \frac{(a_2^2 - a_3^2) B_{23}}{\left[(1+p)(1+\delta) \left\{ 1 + 2 \frac{a_1^2}{a_1^2 + a_2^2} f_R + \left(\frac{a_1 a_2}{a_1^2 + a_2^2} f_R \right)^2 \right\} - 1 \right] a_2^2 + a_3^2} = 0, \quad (3.7)$$

where \bar{a} is the mean radius of the primary. In the generalized pseudo-Newtonian case, the quadrupole term δ is written as

$$\delta = \frac{3}{10} \left\{ 2a_1^2 - \frac{(3R - r_{pseudo})(R - r_{pseudo})}{3R^2} (a_2^2 + a_3^2) \right\} \frac{1}{(R - r_{pseudo})^2}. \quad (3.8)$$

We also have the separation of the binary as

$$R = \frac{E}{E - 2} r_{pseudo}, \quad (3.9)$$

where

$$E \equiv - (1+p)(1+\delta) \left\{ 1 + 2 \frac{a_2^2}{a_1^2 + a_2^2} f_R + \left(\frac{a_1 a_2}{a_1^2 + a_2^2} f_R \right)^2 \right\} - \frac{a_3^2}{a_1^2} + \left\{ \left[(1+p)(1+\delta) \left\{ 1 + 2 \frac{a_1^2}{a_1^2 + a_2^2} f_R + \left(\frac{a_1 a_2}{a_1^2 + a_2^2} f_R \right)^2 \right\} - 1 \right] \frac{a_2^2}{a_1^2} + \frac{a_3^2}{a_1^2} \right\} \frac{(a_1^2 - a_3^2) B_{13}}{(a_2^2 - a_3^2) B_{23}}. \quad (3.10)$$

For the given mass ratio p , mean radius \bar{a}/m_1 , circulation parameter f_R and axial ratio a_3/a_1 , we can determine the axial ratio a_2/a_1 by solving Eq.(3.7) with Eqs.(3.8) and (3.9). Using the axial ratios $(a_2/a_1, a_3/a_1)$, we are able to calculate the orbital angular velocity by Eq.(2.34) and the separation of the binary by Eq.(3.9). The total angular momentum is calculated by Eq.(2.37). Finding the minimum of the total angular momentum, we can determine the location of the ISCO.

When the viscosity inside the primary is so effective that no internal motion exists, $f_R = 0$ in the above equation, i.e. the Roche ellipsoids (REs). While if the primary is in-viscid and $\mathcal{C} = 0$, we have $f_R = -2$, i.e. the irrotational Roche-Riemann ellipsoids (IRREs). Note that if we substitute the Newtonian potential as an interaction potential, Eqs.(2.33) and (2.34) agree with the equations derived by Chandrasekhar [8] in the REs ($f_R = 0$) case and those by Aizenman [15] in the RREs case.

IV. RESULTS

Kochanek [16] and Bildsten & Cutler [17] showed that the internal structure of a coalescing binary neutron star is the irrotational Roche-Riemann ellipsoids (IRREs). However we calculate both the REs and the IRREs for comparison. We show the results in four cases; 1) the REs with $p = 1$ or 0.1, 2) the IRREs with $p = 1$ or 0.1. Results are given in Table.I to Table.VI, where $\tilde{\Omega} = \Omega/\sqrt{\pi\rho_1}$ represents the normalized orbital angular velocity, and \tilde{J} denotes the normalized total angular momentum defined by

$$\tilde{J} = \frac{J_{tot}}{m_1 m_2 (r_s/M_{tot})^{1/2}}. \quad (4.1)$$

\bar{a} is the mean radius of the primary defined by

$$\bar{a} = \left(\frac{m_1}{\frac{4}{3}\pi\rho_1} \right)^{1/3}. \quad (4.2)$$

In Tables I to VI, † means the point of the ISCO defined in this paper, and ‡ does the point of the Roche limit where the Roche limit is defined by the distance of closest approach for equilibrium to be possible [8]. The values in the parentheses show the power of 10.

A. $p = 1$ Case

Fig.2(a) shows \tilde{J} as a function of the normalized separation R/r_s . In Fig.2(a), thin solid, dotted and dashed lines are the REs with \bar{a}/m_1 being 3, 5 and 8, respectively, while thick solid, dotted and dashed lines are the IRREs with \bar{a}/m_1 being 3, 5 and 8, respectively. We defined in §§II.C that the location of the ISCO is the minimum point of \tilde{J} . From Fig.2(a), we see that the separations of the binary at the ISCO in the IRREs case are almost the same as those in the REs case.

Fig.2(b) shows the axial ratios a_2/a_1 and a_3/a_1 as a function of R/r_s . The conventions of lines are the same as those in Fig.2(a). The relation among the length of the axes is $a_1 > a_2 > a_3$ in the REs, while $a_1 > a_3 > a_2$ in the IRREs. In the REs, the tidal force makes the a_1 axis long while it does a_2 and a_3 axes short. The centrifugal force makes a_1 and a_2 axes long. As a result we have $a_1 > a_2 > a_3$. In the IRREs, in addition to the above effects, the Coriolis force caused by the internal motion of the primary exists. This makes a_1 and a_2 axes short, which yields $a_1 > a_3 > a_2$.

From Fig.2(b), it is found that in the IRREs the star with $\bar{a}/m_1 = 3$ reaches the ISCO at the point of $a_2/a_1 \simeq 0.912$ and $a_3/a_1 \simeq 0.918$. On the other hand, the star with $\bar{a}/m_1 = 8$ terminates when $a_2/a_1 \simeq 0.760$ and $a_3/a_1 \simeq 0.792$. This means that the primary with the smaller mean radius reaches the ISCO before the shape of the primary deviates from the sphere considerably. This tendency is the same for the REs.

B. $p = 0.1$ Case

Fig.3(a) shows \tilde{J} as a function of R/r_s . The conventions are the same as those in Fig.2(a) except \bar{a}/m_1 being 3, 5 and 8. From Fig.3(a), we see that all lines with the mean radii in the range of $3 \leq \bar{a}/m_1 \leq 8$ take their minimum at the points near $R/r_s \sim 3.25$. This value is almost the same as the ISCO by Kidder, Will, & Wiseman [7] for $p = 0.1$. This means that when p is much less than 1 and the mean radius of the primary is less than $8m_1$ which corresponds to 17km for $m_1 = 1.4M_\odot$, the size of the primary has little effect on the ISCO.

Fig.3(b) shows the axial ratios a_2/a_1 and a_3/a_1 as a function of R/r_s . The conventions are the same as those in Fig.3(a). We see that the stars with smaller mean radii reach the ISCO even when the deviation from the spherical symmetry is very small. Since the binary system enters an unstable circular orbit before the primary is tidally deformed, the tidal effects are not important. We see that even $\bar{a}/m_1 \sim 8$ the minimum values a_2/a_1 and a_3/a_1 are not small (~ 0.85).

V. DISCUSSIONS

In this section, we discuss the differences between the case of the generalized pseudo-Newtonian potential and that of the Newtonian potential, and between the REs and the IRREs. We will also compare our results with other papers.

A. The Case of $p = 1$

In Fig.4, the separation R_{ISCO}/r_s is shown as a function of \bar{a}/m_1 . Thick lines and thin lines represent the case of the generalized pseudo-Newtonian potential and that of the Newtonian potential, respectively. Solid lines and dotted lines express the case of the IRREs and the REs, respectively. We see that for the Newtonian potential, R_{ISCO}/r_s increases in proportion to \bar{a}/m_1 regardless of types of ellipsoids, while for the generalized pseudo-Newtonian potential, the behavior of R_{ISCO}/r_s changes around $\bar{a}/m_1 \simeq 3.5$.

For $\bar{a}/m_1 \gtrsim 3.5$, R_{ISCO}/r_s increases in proportion to \bar{a}/m_1 as in the case of the Newtonian potential. In this region, the tidal effect dominates the system and the effects of the general relativity become less important. In conclusion, for $\bar{a}/m_1 \gtrsim 3.5$, the tidal effect dominates the stability of the binary system and for $\bar{a}/m_1 \lesssim 3.5$, the binary system is dominated by the relativistic effect, i.e. the fact that the interaction potential has an unstable orbit. From Fig.4 it is also found that the location of the ISCOs in the IRREs case is not so different from that in the REs case for the same \bar{a}/m_1 .

The orbital frequency of the IRREs at the ISCO for $m_1 = 1.4M_\odot$ and $\bar{a}/m_1 = 5$ is estimated from $\tilde{\Omega}$ in Table.IV as

$$\Omega_{ISCO} = 495 \text{ [Hz]}. \quad (5.1)$$

This value is smaller than that in the Newtonian potential case ($\Omega_{ISCO}^{Newton} = 599 \text{ [Hz]}$).

B. The Case of $p = 0.1$

If we consider the primary as the neutron star of mass $1.4M_\odot$, then, the secondary is regarded as the black hole of mass $14M_\odot$. R_{ISCO}/r_s is shown as a function of \bar{a}/m_1 in Fig.5. For the Newtonian potential, R_{ISCO}/r_s increases in proportion to \bar{a}/m_1 like the case of $p = 1$. For the generalized pseudo-Newtonian potential, in the range of \bar{a}/m_1 of Fig.5, R_{ISCO}/r_s converges to the value 3.25 obtained by Kidder, Will, & Wiseman [7]. This is because the existence of the unstable orbit in the generalized pseudo-Newtonian potential influences R_{ISCO}/r_s , and this effect dominates when the radius of the primary is small. This is clearer for the small mass ratio p . Therefore if p is small, for the range of the radius ($3 \leq \bar{a}/m_1 \leq 8$) relevant to the neutron star, the effect of the neutron star's size is very small. This comes essentially from the fact that the Newtonian estimate of the Roche radius is smaller than the radius of the ISCO.

One can estimate the orbital frequency of the IRREs at the ISCO for $m_1 = 1.4M_\odot$ and $\bar{a}/m_1 = 5$ from $\tilde{\Omega}$ in Table.V as

$$\Omega_{ISCO} = 187 \text{ [Hz]}. \quad (5.2)$$

C. Comparison with Other Works

Kidder, Will, & Wiseman [7] studied the motion of the point-particle binary systems using *hybrid Schwarzschild second post-Newtonian equation of motion*, and obtained the separation at the ISCO (r_{ISCO}) expressed by

$$\frac{r_{ISCO}}{M_{tot}} \simeq 6 + 7.49\eta - 20.8\eta^2 + 29.3\eta^3 \quad (5.3)$$

where

$$\eta = \frac{m_1 m_2}{M_{tot}^2}. \quad (5.4)$$

Table.VII shows the comparison of Eq.(5.3) with our results for $\bar{a}/m_1 = 5$. It is found that for $p = 0.1$, the finite size effect is not important because the primary is much lighter than the secondary, so that the results are almost the same as [7]. On the other hand, when $p = 1$ the finite size of the primary increases the separation at the ISCO by the general relativistic and tidal effects.

Lai, Rasio, & Shapiro [18], discussed the relativistic effects on the binary system for compressible Darwin ellipsoids using a simple approximate model [19]. The Darwin ellipsoids are the equilibrium configurations constructed by two identical synchronized finite-size stars including the mutual tidal interactions. In their approach the effects of general relativity and the Newtonian tidal interactions for finite-size compressible stars are combined by hand. While we formulated the problem using arbitrary interaction potentials of the secondary for the incompressible primary. We adopted the semi-relativistic potential called the generalized pseudo-Newtonian potential to mimic the general relativistic effects of gravitation. We solved the equilibria of the REs and the IRREs in this potential. Their results and ours are compared in Table.VIII, where r_m expresses the minimum separation obtained by Lai, Rasio, & Shapiro [18]. From this table, we see that both results agree rather well inspite of different approaches and approximations.

ACKNOWLEDGMENTS

KT would like to thank H. Sato, K. Nakao and M. Shibata for useful discussions and continuous encouragement. This work was in part supported by a Grant-in-Aid for Basic Research of Ministry of Education, Culture, Science and Sports (08NP0801).

REFERENCES

- [1] A. Abramovici, et al. *Science* **256** (1992), 325.
- [2] C. Bradaschia, et al. *Nucl. Instrum. and Methods* **A289** (1990), 518.
- [3] J. Hough, in *Proceedings of the Sixth Marcel Grossmann Meeting*, edited by H. Sato and T. Nakamura (World Scientific, Singapore, 1992), p.192.
- [4] K. Kuroda et al. in *Proceedings of International Conference on Gravitational Waves: Sources and Detectors*, Pisa, Italy, March 19-23, 1996 (in press).
- [5] C. Cutler and E. E. Flanagan, *Phys. Rev.* **D49** (1994), 2658.
- [6] C. Cutler, et al. *Phys. Rev. Lett.* **70** (1993), 2984.
- [7] L. E. Kidder, C. M. Will, and A. G. Wiseman, *Class. Quantum Gravity* **9** (1992), L125.
L. E. Kidder, C. M. Will, and A. G. Wiseman, *Phys. Rev.* **D47** (1993), 3281.
- [8] S. Chandrasekhar, *Ellipsoidal Figures of Equilibrium*, (Yale University Press, New Haven, 1969).
- [9] D. Lai, F. A. Rasio, and S. L. Shapiro, *Astrophys. J. Suppl.* **88** (1993), 205.
- [10] D. Lai, F. A. Rasio, and S. L. Shapiro, *Astrophys. J.* **423** (1994), 344.
D. Lai, F. A. Rasio, and S. L. Shapiro, *Astrophys. J.* **437** (1994), 742.
- [11] T. Nakamura, in *Proceedings of the Seventh Marcel Grossmann Meeting*, Stanford, July, 1994 (in press).
- [12] J. R. Wilson and G. J. Mathews, *Phys. Rev. Lett.* **75** (1995), 4161.
J. R. Wilson, G. J. Mathews, and P. Marroetti, *preprint*, gr-qc/9601017 (1996).
- [13] M. Shibata, *preprint* (1995).
- [14] B. Paczyński and P. J. Wiita, *Astron. Astrophys.* **88** (1980), 23.
- [15] M. L. Aizenman, *Astrophys. J.* **153** (1968), 511.
- [16] C. S. Kochanek, *Astrophys. J.* **398** (1992), 234.
- [17] L. Bildsten and C. Cutler, *Astrophys. J.* **400** (1992), 175.
- [18] D. Lai, F. A. Rasio, and S. L. Shapiro, *Astrophys. J.* **420** (1994), 811.
- [19] D. Lai, F. A. Rasio, and S. L. Shapiro, *Astrophys. J.* **406** (1993), L63.

TABLE CAPTIONS

Table.I. Equilibrium Sequences of the Roche ellipsoids (REs) and the irrotational Roche Riemann ellipsoids (IRREs) with $p = 1$ and $\bar{a}/m_1 = 3$.

Table.II. Equilibrium Sequences of the REs and the IRREs with $p = 1$ and $\bar{a}/m_1 = 5$.

Table.III. Equilibrium Sequences of the REs and the IRREs with $p = 1$ and $\bar{a}/m_1 = 8$.

Table.IV. Equilibrium Sequences of the REs and the IRREs with $p = 0.1$ and $\bar{a}/m_1 = 3$.

Table.V. Equilibrium Sequences of the REs and the IRREs with $p = 0.1$ and $\bar{a}/m_1 = 5$.

Table.VI. Equilibrium Sequences of the REs and the IRREs with $p = 0.1$ and $\bar{a}/m_1 = 8$.

Table.VII. Comparison of our results ($\bar{a}/m_1 = 5$) with that of Kidder, Will, & Wiseman[7] in the cases of $p = 1$ and 0.1.

Table.VIII. Comparison of our results ($p = 1$) with that of Lai, Rasio, & Shapiro[18] in the cases of $\bar{a}/m_1 = 5$ and 8.

TABLES

$p = 1$									
$\bar{a}/m_1 = 3$									
Roche Sequences					Irrotational Roche-Riemann Sequences				
a_3/a_1	a_2/a_1	Ω^2	\tilde{J}	R/r_s	a_3/a_1	a_2/a_1	Ω^2	\tilde{J}	R/r_s
0.950	0.966	1.87(-2)	2.97	4.75	0.950	0.948	2.69(-2)	2.87	4.31
					0.918	0.912	4.10(-2)	2.86	3.87 †
0.912	0.939	3.19(-2)	2.94	4.13 †					
0.900	0.929	3.59(-2)	2.94	4.00	0.900	0.891	4.81(-2)	2.86	3.72
0.850	0.889	5.19(-2)	2.97	3.65	0.850	0.833	6.53(-2)	2.88	3.46
0.800	0.847	6.67(-2)	3.01	3.44	0.800	0.773	7.92(-2)	2.92	3.31
0.750	0.801	8.03(-2)	3.05	3.30	0.750	0.715	9.02(-2)	2.95	3.22
0.700	0.754	9.23(-2)	3.10	3.21	0.700	0.657	9.87(-2)	3.00	3.17
0.650	0.704	1.03(-1)	3.15	3.14	0.650	0.601	1.05(-1)	3.04	3.14
0.600	0.652	1.11(-1)	3.20	3.10	0.600	0.547	1.09(-1)	3.09	3.12
					0.577	0.524	1.11(-1)	3.12	3.12 ‡
0.550	0.599	1.17(-1)	3.26	3.08	0.550	0.496	1.12(-1)	3.15	3.12
0.514	0.560	1.20(-1)	3.30	3.07 ‡					
0.500	0.544	1.21(-1)	3.32	3.07	0.500	0.447	1.12(-1)	3.21	3.14
0.450	0.489	1.22(-1)	3.38	3.09	0.450	0.400	1.11(-1)	3.28	3.17
0.400	0.433	1.19(-1)	3.45	3.12	0.400	0.354	1.07(-1)	3.36	3.21
0.350	0.376	1.14(-1)	3.53	3.18	0.350	0.310	1.02(-1)	3.45	3.28
0.300	0.320	1.05(-1)	3.63	3.27	0.300	0.267	9.33(-2)	3.56	3.37
0.250	0.264	9.17(-2)	3.75	3.41	0.250	0.225	8.23(-2)	3.69	3.51
0.200	0.209	7.53(-2)	3.90	3.62	0.200	0.182	6.83(-2)	3.86	3.72

TABLE I.

$p = 1$									
$\bar{a}/m_1 = 5$									
Roche Sequences					Irrotational Roche-Riemann Sequences				
a_3/a_1	a_2/a_1	Ω^2	\tilde{J}	R/r_s	a_3/a_1	a_2/a_1	Ω^2	\tilde{J}	R/r_s
0.950	0.967	1.97(-2)	3.30	7.24	0.950	0.947	2.90(-2)	3.12	6.47
0.900	0.931	3.81(-2)	3.18	5.99	0.900	0.890	5.25(-2)	3.02	5.48
0.850	0.892	5.56(-2)	3.15	5.40	0.850	0.831	7.15(-2)	2.99	5.05
					0.832	0.810	7.73(-2)	2.99	4.95 †
0.828	0.874	6.29(-2)	3.15	5.22 †					
0.800	0.850	7.19(-2)	3.15	5.04	0.800	0.771	8.67(-2)	2.99	4.81
0.750	0.806	8.68(-2)	3.17	4.81	0.750	0.711	9.85(-2)	3.01	4.66
0.700	0.759	1.00(-1)	3.20	4.64	0.700	0.653	1.08(-1)	3.04	4.57
0.650	0.709	1.12(-1)	3.24	4.53	0.650	0.597	1.14(-1)	3.08	4.52
0.600	0.657	1.21(-1)	3.28	4.46	0.600	0.543	1.19(-1)	3.14	4.50
					0.582	0.524	1.20(-1)	3.16	4.50 ‡
0.550	0.604	1.28(-1)	3.34	4.42	0.550	0.492	1.21(-1)	3.20	4.51
0.513	0.564	1.31(-1)	3.38	4.41 ‡					
0.500	0.549	1.32(-1)	3.40	4.41	0.500	0.443	1.21(-1)	3.28	4.53
0.450	0.493	1.33(-1)	3.48	4.44	0.450	0.396	1.20(-1)	3.36	4.58
0.400	0.436	1.30(-1)	3.57	4.50	0.400	0.351	1.15(-1)	3.47	4.66
0.350	0.378	1.23(-1)	3.68	4.60	0.350	0.308	1.09(-1)	3.59	4.77
0.300	0.321	1.13(-1)	3.81	4.75	0.300	0.265	9.96(-2)	3.75	4.94
0.250	0.265	9.85(-2)	3.98	4.99	0.250	0.223	8.75(-2)	3.94	5.17
0.200	0.209	8.03(-2)	4.22	5.34	0.200	0.182	7.23(-2)	4.19	5.51

TABLE II.

$p = 1$									
$\bar{a}/m_1 = 8$									
Roche Sequences					Irrotational Roche-Riemann Sequences				
a_3/a_1	a_2/a_1	Ω^2	\tilde{J}	R/r_s	a_3/a_1	a_2/a_1	Ω^2	\tilde{J}	R/r_s
0.950	0.968	2.02(-2)	3.82	11.00	0.950	0.947	3.04(-2)	3.56	9.71
0.900	0.932	3.95(-2)	3.61	8.98	0.900	0.890	5.53(-2)	3.37	8.13
0.850	0.894	5.78(-2)	3.54	8.03	0.850	0.830	7.54(-2)	3.30	7.44
0.800	0.853	7.50(-2)	3.51	7.46	0.800	0.769	9.13(-2)	3.28	7.06
					0.792	0.760	9.35(-2)	3.28	7.02 †
0.774	0.830	8.34(-2)	3.51	7.24 †					
0.750	0.809	9.09(-2)	3.51	7.07	0.750	0.709	1.04(-1)	3.29	6.84
0.700	0.762	1.05(-1)	3.53	6.81	0.700	0.651	1.13(-1)	3.31	6.70
0.650	0.712	1.17(-1)	3.56	6.63	0.650	0.595	1.20(-1)	3.36	6.62
0.600	0.661	1.27(-1)	3.60	6.51	0.600	0.541	1.24(-1)	3.42	6.59
					0.584	0.524	1.25(-1)	3.44	6.59 ‡
0.550	0.607	1.35(-1)	3.66	6.45	0.550	0.490	1.27(-1)	3.49	6.60
0.513	0.566	1.38(-1)	3.72	6.43 ‡					
0.500	0.552	1.39(-1)	3.74	6.44	0.500	0.441	1.27(-1)	3.59	6.64
0.450	0.495	1.40(-1)	3.83	6.48	0.450	0.394	1.25(-1)	3.70	6.72
0.400	0.438	1.37(-1)	3.94	6.57	0.400	0.349	1.20(-1)	3.83	6.85
0.350	0.380	1.30(-1)	4.08	6.74	0.350	0.306	1.13(-1)	3.99	7.03
0.300	0.322	1.18(-1)	4.26	6.99	0.300	0.264	1.04(-1)	4.19	7.29
0.250	0.265	1.03(-1)	4.49	7.37	0.250	0.223	9.06(-2)	4.45	7.66
0.200	0.210	8.33(-2)	4.80	7.94	0.200	0.181	7.47(-2)	4.78	8.22

TABLE III.

$p = 0.1$									
$\bar{a}/m_1 = 3$									
Roche Sequences					Irrotational Roche-Riemann Sequences				
a_3/a_1	a_2/a_1	Ω^2	\tilde{J}	R/r_s	a_3/a_1	a_2/a_1	Ω^2	\tilde{J}	R/r_s
					0.992	0.992	2.42(-3)	2.70	3.26 †
0.990	0.992	2.39(-3)	2.71	3.27 †					
0.950	0.959	9.94(-3)	2.85	2.35	0.950	0.949	1.17(-2)	2.89	2.27
0.900	0.914	1.80(-2)	3.02	2.08	0.900	0.896	2.04(-2)	3.06	2.03
0.850	0.868	2.51(-2)	3.16	1.96	0.850	0.843	2.76(-2)	3.19	1.93
0.800	0.821	3.12(-2)	3.26	1.88	0.800	0.789	3.35(-2)	3.29	1.86
0.750	0.772	3.65(-2)	3.35	1.84	0.750	0.735	3.84(-2)	3.37	1.82
0.700	0.722	4.10(-2)	3.42	1.80	0.700	0.682	4.23(-2)	3.43	1.79
0.650	0.672	4.47(-2)	3.48	1.78	0.650	0.629	4.53(-2)	3.48	1.77
0.600	0.621	4.75(-2)	3.52	1.76	0.600	0.577	4.74(-2)	3.51	1.76
0.550	0.569	4.93(-2)	3.56	1.75	0.550	0.526	4.86(-2)	3.54	1.76
					0.525	0.501	4.89(-2)	3.55	1.76 ‡
0.500	0.517	5.02(-2)	3.58	1.75 ‡	0.500	0.476	4.90(-2)	3.55	1.76
0.450	0.465	5.01(-2)	3.59	1.75	0.450	0.427	4.85(-2)	3.56	1.76
0.400	0.412	4.89(-2)	3.58	1.76	0.400	0.379	4.70(-2)	3.55	1.78
0.350	0.360	4.66(-2)	3.57	1.78	0.350	0.331	4.46(-2)	3.54	1.79
0.300	0.308	4.29(-2)	3.54	1.81	0.300	0.284	4.11(-2)	3.51	1.82
0.250	0.255	3.80(-2)	3.49	1.85	0.250	0.238	3.64(-2)	3.46	1.86
0.200	0.204	3.17(-2)	3.42	1.92	0.200	0.192	3.05(-2)	3.40	1.93

TABLE IV.

$p = 0.1$									
$\bar{a}/m_1 = 5$									
Roche Sequences					Irrotational Roche-Riemann Sequences				
a_3/a_1	a_2/a_1	Ω^2	\tilde{J}	R/r_s	a_3/a_1	a_2/a_1	Ω^2	\tilde{J}	R/r_s
					0.962	0.961	1.10(-2)	2.71	3.28 †
0.953	0.962	1.07(-2)	2.71	3.30 †					
0.950	0.960	1.14(-2)	2.71	3.25	0.950	0.949	1.38(-2)	2.71	3.09
0.900	0.917	2.12(-2)	2.75	2.79	0.900	0.896	2.47(-2)	2.75	2.70
0.850	0.872	3.00(-2)	2.79	2.58	0.850	0.841	3.38(-2)	2.80	2.51
0.800	0.825	3.78(-2)	2.83	2.45	0.800	0.787	4.14(-2)	2.84	2.41
0.750	0.777	4.47(-2)	2.87	2.37	0.750	0.732	4.76(-2)	2.88	2.34
0.700	0.728	5.06(-2)	2.91	2.31	0.700	0.678	5.17(-2)	2.90	2.30
0.650	0.677	5.55(-2)	2.94	2.27	0.650	0.624	5.64(-2)	2.93	2.26
0.600	0.626	5.92(-2)	2.97	2.24	0.600	0.572	5.90(-2)	2.95	2.24
0.550	0.574	6.18(-2)	2.99	2.23	0.550	0.521	6.05(-2)	2.97	2.24
					0.528	0.498	6.08(-2)	2.98	2.24 ‡
0.500	0.521	6.30(-2)	3.00	2.22	0.500	0.471	6.09(-2)	2.98	2.24
0.497	0.518	6.31(-2)	3.00	2.22 ‡					
0.450	0.469	6.29(-2)	3.02	2.22	0.450	0.422	6.02(-2)	2.99	2.25
0.400	0.416	6.13(-2)	3.02	2.24	0.400	0.374	5.82(-2)	3.00	2.27
0.350	0.362	5.82(-2)	3.03	2.27	0.350	0.327	5.50(-2)	3.00	2.30
0.300	0.309	5.34(-2)	3.02	2.32	0.300	0.281	5.04(-2)	3.00	2.35
0.250	0.257	4.69(-2)	3.02	2.39	0.250	0.236	4.44(-2)	3.00	2.42
0.200	0.204	3.88(-2)	3.01	2.47	0.200	0.190	3.69(-2)	3.00	2.53

TABLE V.

$p = 0.1$									
$\bar{a}/m_1 = 8$									
Roche Sequences					Irrotational Roche-Riemann Sequences				
a_3/a_1	a_2/a_1	Ω^2	\tilde{J}	R/r_s	a_3/a_1	a_2/a_1	Ω^2	\tilde{J}	R/r_s
0.950	0.961	1.23(-2)	2.82	4.61	0.950	0.949	1.53(-2)	2.78	4.34
0.900	0.919	2.34(-2)	2.75	3.88	0.900	0.895	2.80(-2)	2.73	3.70
0.850	0.874	3.35(-2)	2.73	3.53	0.850	0.840	3.86(-2)	2.72	3.41
					0.849	0.840	3.87(-2)	2.72	3.41 †
0.832	0.858	3.69(-2)	2.73	3.45 †					
0.800	0.828	4.27(-2)	2.74	3.32	0.800	0.785	4.76(-2)	2.72	3.24
0.750	0.781	5.09(-2)	2.74	3.19	0.750	0.729	5.49(-2)	2.73	3.13
0.700	0.732	5.80(-2)	2.75	3.09	0.700	0.674	6.07(-2)	2.74	3.06
0.650	0.681	6.39(-2)	2.77	3.02	0.650	0.620	6.51(-2)	2.75	3.01
0.600	0.630	6.85(-2)	2.78	2.97	0.600	0.568	6.82(-2)	2.77	2.98
0.550	0.578	7.17(-2)	2.79	2.95	0.550	0.516	6.99(-2)	2.78	2.97
					0.529	0.496	7.02(-2)	2.78	2.97 ‡
0.500	0.525	7.33(-2)	2.81	2.94	0.500	0.466	7.03(-2)	2.79	2.97
0.494	0.519	7.33(-2)	2.81	2.94 ‡					
0.450	0.472	7.32(-2)	2.82	2.94	0.450	0.418	6.93(-2)	2.81	2.98
0.400	0.418	7.13(-2)	2.84	2.97	0.400	0.371	6.69(-2)	2.82	3.02
0.350	0.364	6.75(-2)	2.85	3.02	0.350	0.324	6.31(-2)	2.84	3.07
0.300	0.311	6.17(-2)	2.87	3.09	0.300	0.279	5.76(-2)	2.86	3.14
0.250	0.258	5.39(-2)	2.90	3.21	0.250	0.234	5.05(-2)	2.89	3.26
0.200	0.205	4.41(-2)	2.93	3.38	0.200	0.189	4.17(-2)	2.93	3.44

TABLE VI.

	p	0.1	1
[7]'s results	r_{ISCO}/M_{tot}	6.5	7.0
Our results	R_{ISCO}^{RE}/M_{tot}	6.6	10.4
Our results	R_{ISCO}^{IRRE}/M_{tot}	6.6	9.9

TABLE VII.

$p = 1$			
	\bar{a}/m_1	5	8
[18]'s results	r_m/M_{tot}	8.5	12
Our results	R_{ISCO}^{RE}/M_{tot}	10.4	14.5
Our results	R_{ISCO}^{IRRE}/M_{tot}	9.9	14.0

TABLE VIII.

FIGURE CAPTIONS

Fig.1(a). The effective potentials of a test particle in the Schwarzschild metric (left) and the pseudo-Newtonian potential (right) as a function of the normalized distance R/r_s . The vertical axes denote $\Psi_{Sch} = \sqrt{\left(1 - \frac{2M}{R}\right) \left(\frac{J_{Sch}^2}{R^2} + 1\right)} - 1$ and $\Psi_{pseudo} = -\frac{M}{R-r_s} + \frac{J_{pseudo}^2}{2R^2}$, respectively. The dots express the place of circular orbits. The value of the effective potential of the Schwarzschild black hole at the infinity is shifted to zero.

Fig.1(b). The fractional deviation of the circular orbits of the pseudo-Newtonian potential from those of the Schwarzschild effective potential as a function of the angular momentum. Circular orbits with different angular momentum related as $J_{pseudo} = \left(\frac{9}{8}\right)^{1/2} J_{Sch}$ are compared (see text).

Fig.2(a). The total angular momentum $\tilde{J} = J_{tot}/\{m_1 m_2 (r_s/M_{tot})^{1/2}\}$ of the equilibrium sequence as a function of R/r_s in the case that the mass ratio is $p = 1$. Thin and thick lines express the REs and the IRREs cases, respectively. Solid, dotted, and dashed lines denote $\bar{a}/m_1 = 3, 5$ and 8 , respectively.

Fig.2(b). The axial ratios a_2/a_1 and a_3/a_1 of the equilibrium sequence as a function of R/r_s in the case of the mass ratio $p = 1$. The top figure represents a_2/a_1 , and the bottom does a_3/a_1 . The conventions are the same as in Fig.2(a).

Fig.3(a). The total angular momentum \tilde{J} of the equilibrium sequence as a function of R/r_s in the case of $p = 0.1$. The region around the minimum of the lines is magnified and shown in the upper right corner. The conventions are the same as in Fig.2(a).

Fig.3(b). The axial ratios a_2/a_1 and a_3/a_1 of the equilibrium sequence as a function of R/r_s in the case of $p = 0.1$. The top figure represents a_2/a_1 , and the bottom does a_3/a_1 . The conventions are the same as in Fig.2(a).

Fig.4. The relation between the mean radius of the primary \bar{a}/m_1 and the separation of the binary R_{ISCO}/r_s at the ISCO in the case of $p = 1$. Thin lines denote the case of the Newtonian potential as an interaction potential, and thick lines denote the case of the generalized pseudo-Newtonian potential. The solid and dotted lines represent the IRREs and the REs, respectively.

Fig.5 The relation between the mean radius of the primary \bar{a}/m_1 and the separation of the binary R_{ISCO}/r_s at the ISCO in the case of $p = 0.1$. The conventions are the same as in Fig.4.

FIGURES

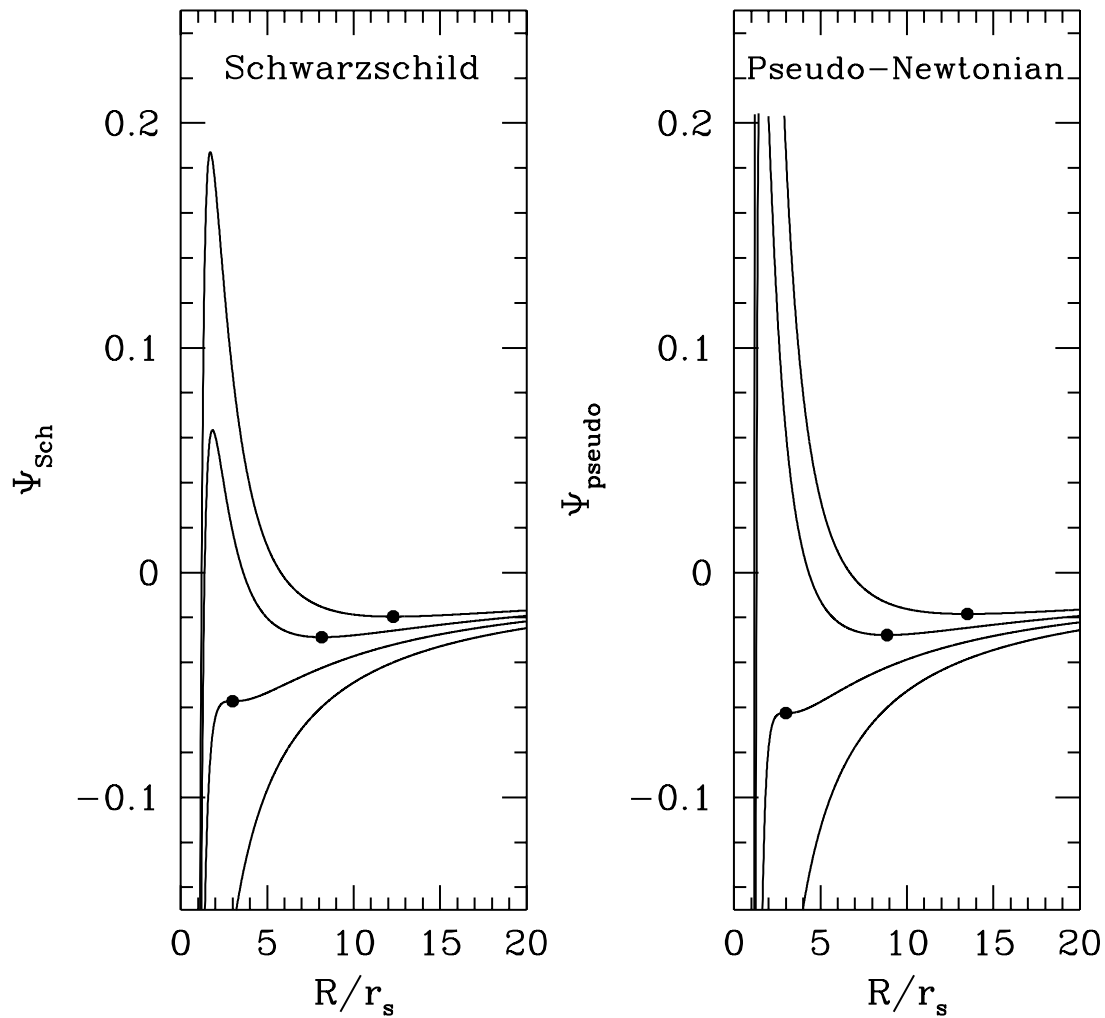


Fig.1(a)

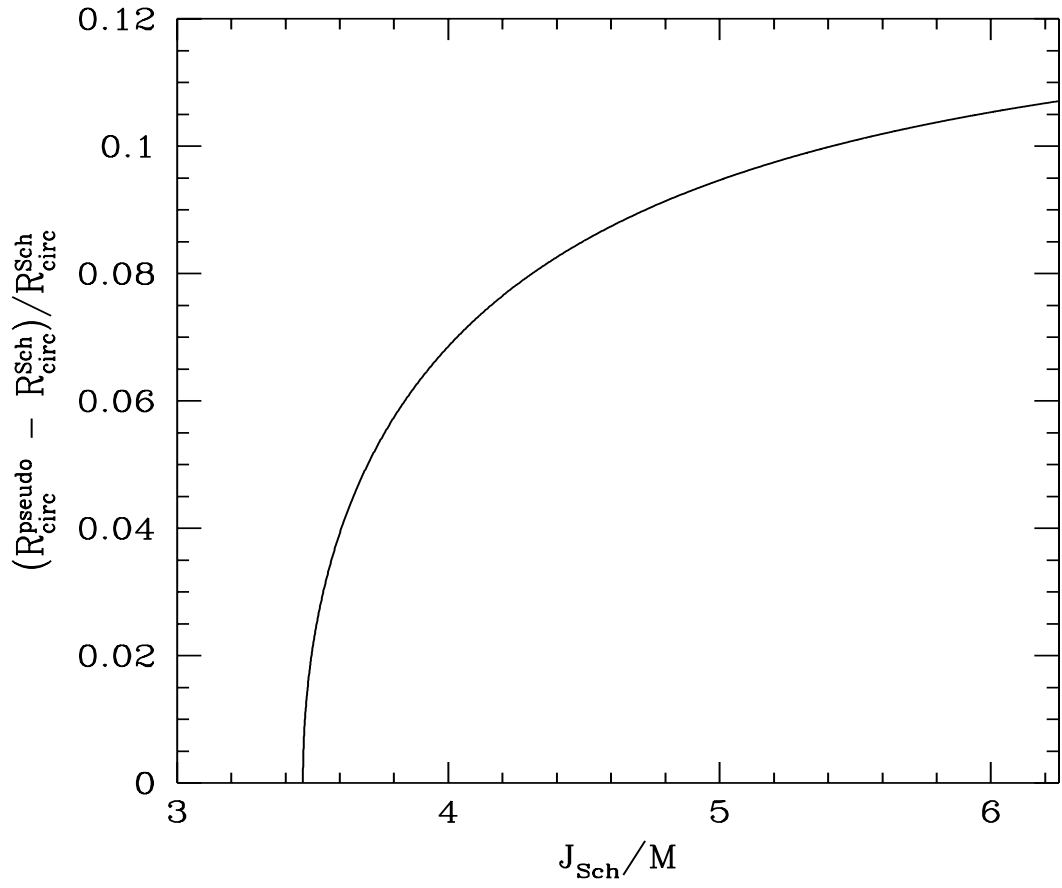


Fig.1(b)

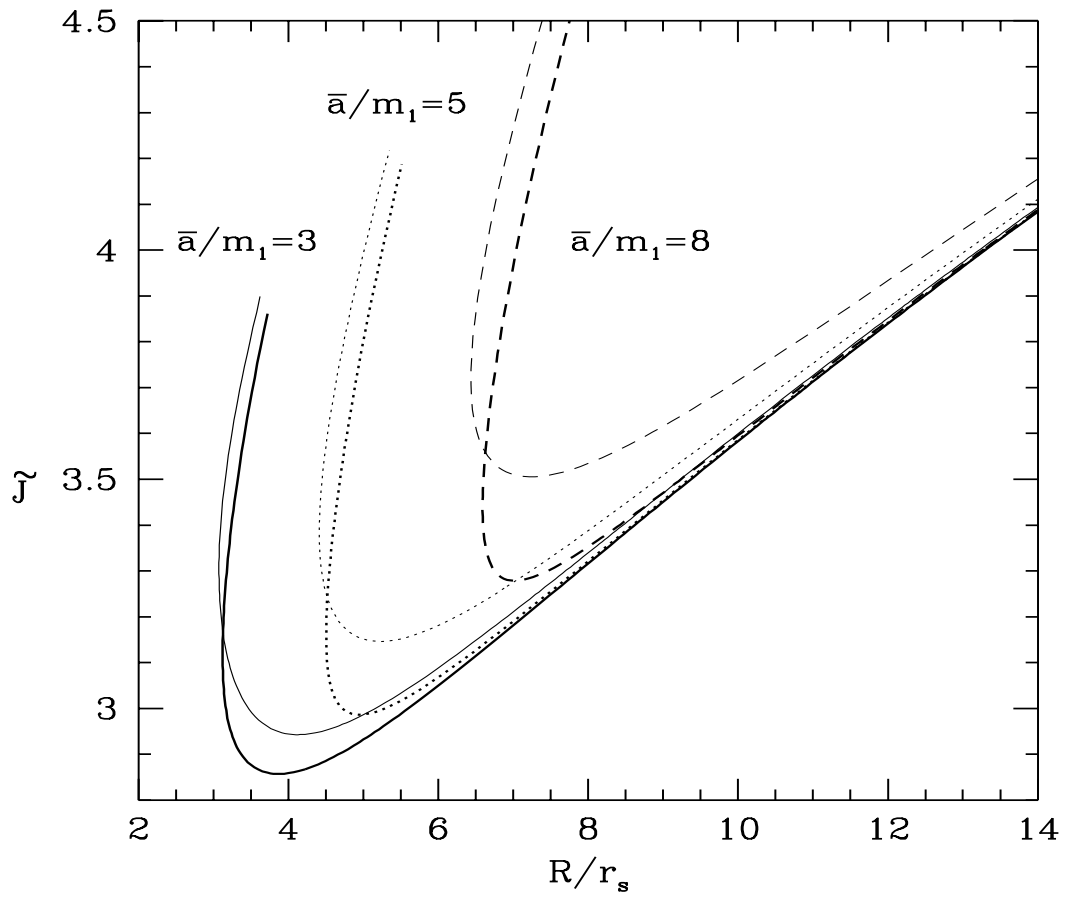


Fig.2(a)

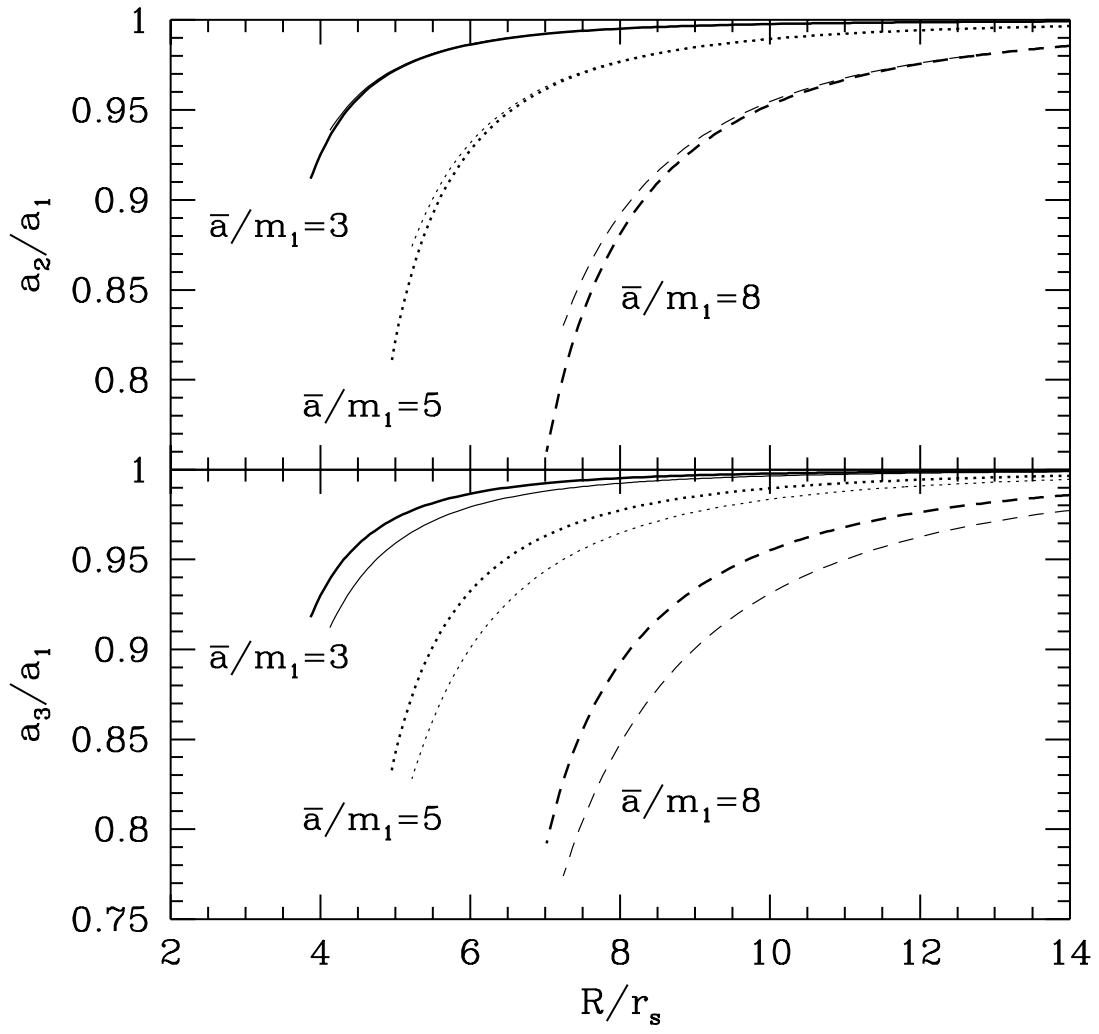


Fig.2(b)

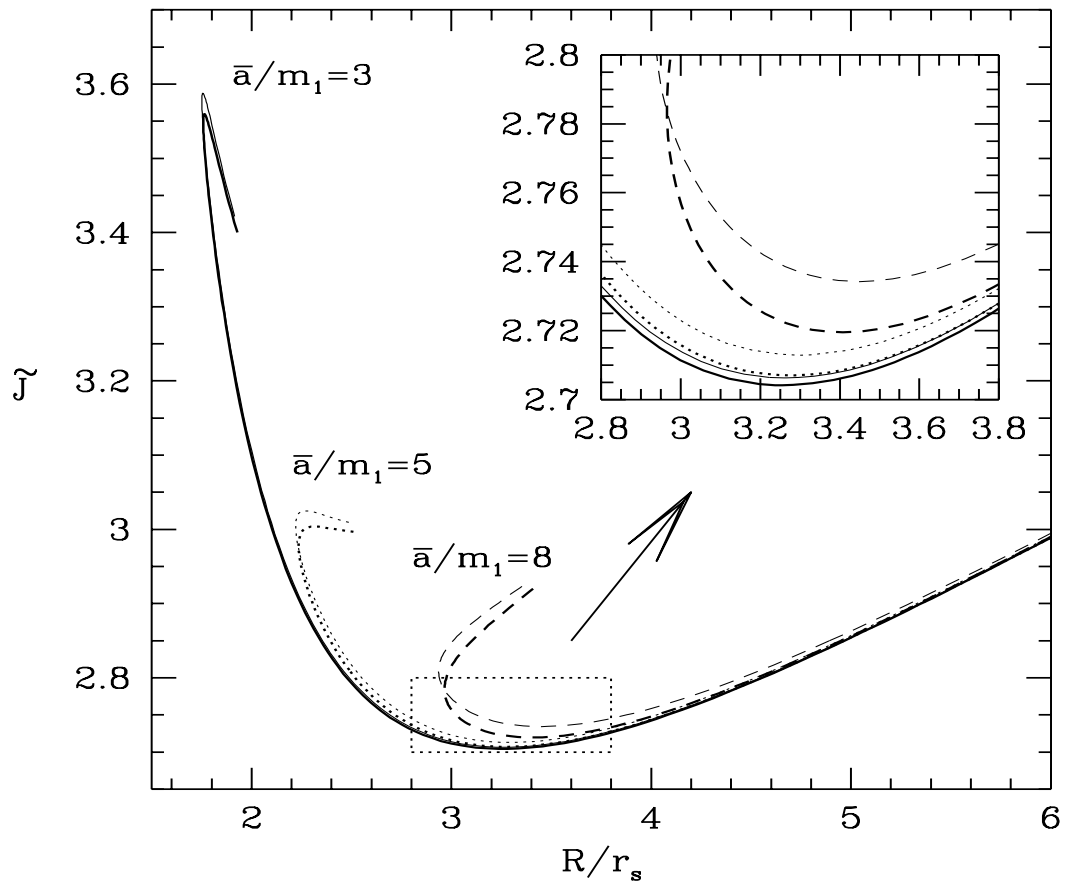


Fig.3(a)

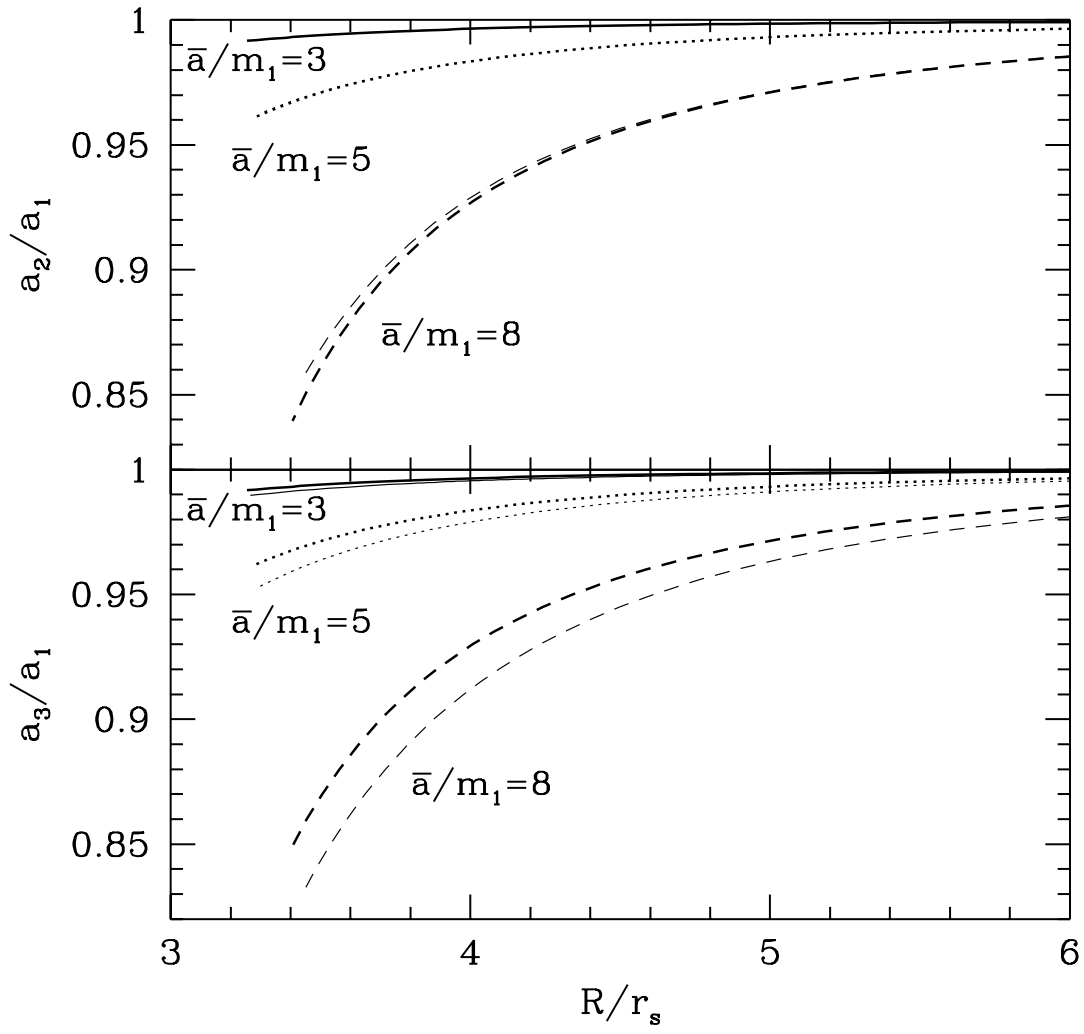


Fig.3(b)

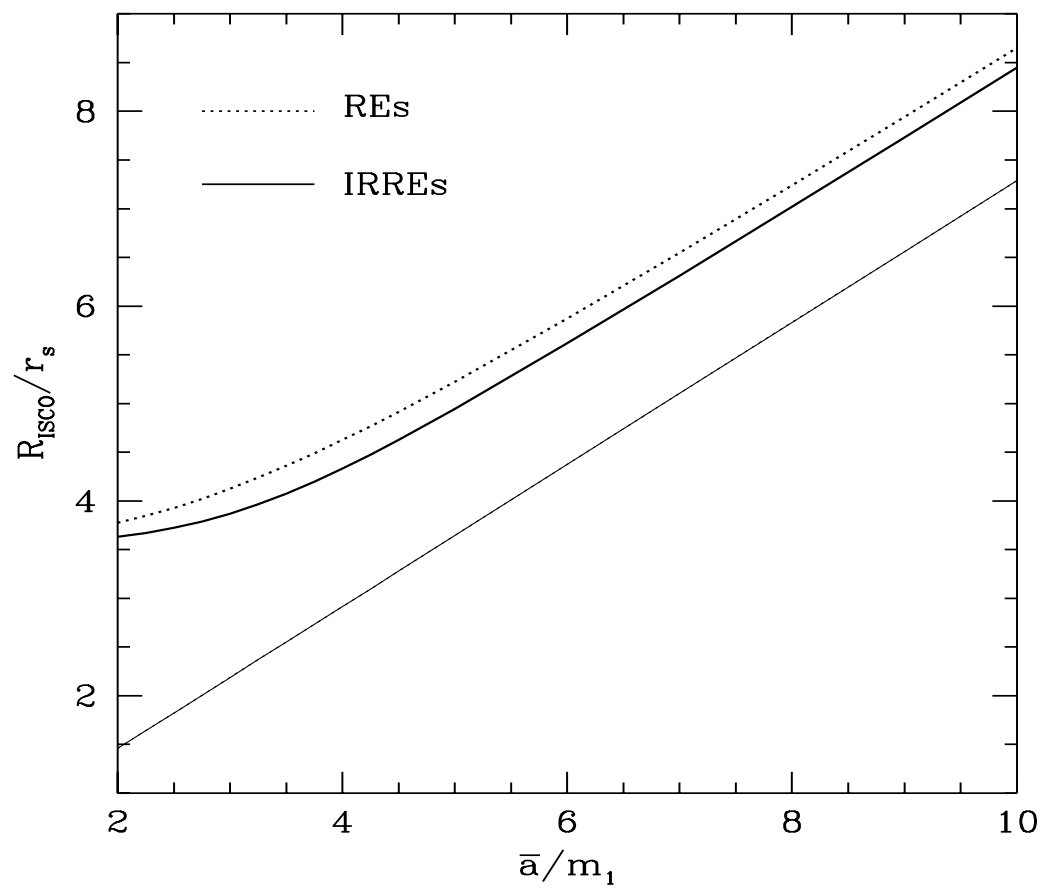


Fig.4

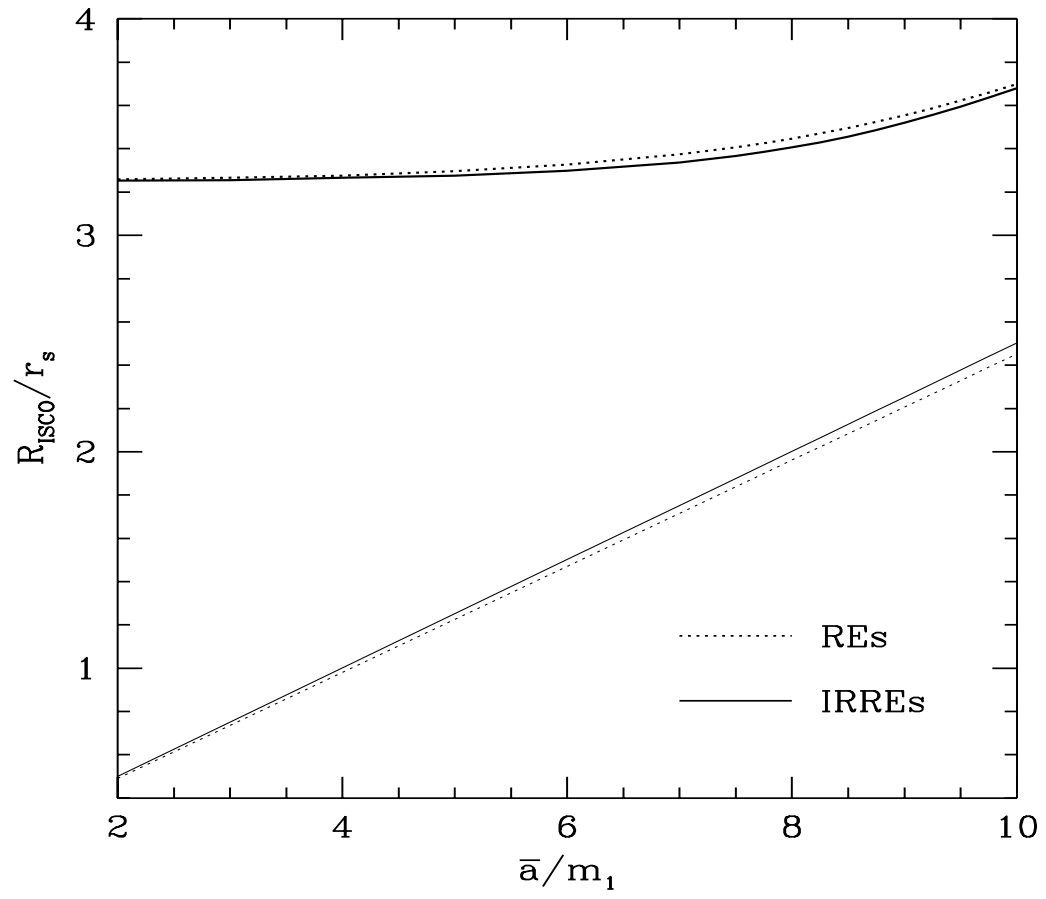


Fig.5